applied sciences

MDPI

Article

Numerical Simulation of the Mechanical Behavior of Fiber-Reinforced Cement Composites Subjected Dynamic Loading

Nikita Belyakov [1], Olga Smirnova [1,*], Aleksandr Alekseev [1] and Hongbo Tan [2]

[1] Department of Constructing Mining Enterprises and Underground Structures, Saint Petersburg Mining University, 199106 Saint Petersburg, Russia; nikebel87@gmail.com (N.B.); Alekseev_av2@pers.spmi.ru (A.A.)
[2] State Key Laboratory of Silicate Materials for Architectures, Wuhan University of Technology, Wuhan 430070, China; thbwhut@whut.edu.cn
* Correspondence: smirnovaolgam@rambler.ru

Abstract: The problem of damage accumulation in fiber-reinforced concrete to structures supporting underground workings and tunnel linings against dynamic loading is insufficiently studied. The mechanical properties were determined and the mechanism of destruction of fiber-reinforced concrete with different reinforcement parameters is described. The parameters of the Concrete Damaged Plasticity model for fiber-reinforced concrete at different reinforcement properties are based on the results of lab experiments. Numerical simulation of the composite concrete was performed in the Simulia Abaqus software package (Dassault Systemes, Vélizy-Villacoublay, France). Modeling of tunnel lining based on fiber-reinforced concrete was performed under seismic loading.

Keywords: Simulia Abaqus; finite element method; concrete cracking; seismic loading; tunnel lining

Citation: Belyakov, N.; Smirnova, O.; Alekseev, A.; Tan, H. Numerical Simulation of the Mechanical Behavior of Fiber-Reinforced Cement Composites Subjected Dynamic Loading. *Appl. Sci.* **2021**, *11*, 1112. https://doi.org/10.3390/app11031112

Received: 17 December 2020
Accepted: 18 January 2021
Published: 26 January 2021

1. Introduction

In recent years, a significant number of scientific papers have been devoted to the development of new compositions of cement matrices and the use of modified multicomponent fibers in concrete compositions for static and dynamic loads [1–4].

Determining the mechanical properties of fiber-reinforced cement composites under dynamic loading, establishing correlations among their composition, structure and properties, justifying the correct mathematical model and determining its parameters represent a complex problem at the moment. If this problem is solved, the efficiency of building structures operating under dynamic loading can be improved, i.e., with respect to an economic point of view because of lowering material consumption and correct results of analytical and numerical approaches.

The Finite Element Method (FEM) is commonly used in determining the non-linear relationship of force-displacement and following crack development in reinforced concrete [5,6]. The analytical model of plastic behavior of polymeric fiber and concrete is quite complicated [7,8]. In this study, the commercially available Simulia Abaqus software package was used. Using Abaqus for performing the computational experiment makes it possible to reproduce the phenomenon in the most detailed way, including visualization for analysis and comparison of the obtained numerical data with experimental results [9–13].

The analysis of scientific publications in the field of research showed that problem of damage accumulation in concrete and fiber-reinforced concrete tunnel linings under dynamic loading is insufficiently studied [14–17].

The aim of the paper is to substantiate the mechanism of damage accumulation in the tunnel lining with the circular outline using the model of plastic behavior of concrete for the evolution of damage.

The scientific significance of the paper is related to the development of theoretical ideas about the mechanics of degradation of fiber-reinforced concrete based on laboratory test results as well as to the improvement of mathematical modeling of the material behavior using complex models of continuum mechanics.

2. Materials and Methods

2.1. The Studied Materials

Concretes of B15 and B25 compressive strength classes were studied. These concretes are made in accordance with the regulatory documents in force in Russia and have mechanical properties indicated in Table 1.

Table 1. Basic mechanical properties of the studied materials.

Material	Young's Modulus, GPa	Compressive Strength, MPa	Tensile Strength, MPa
B15 concrete strength class	24	8.5	0.75
B25 concrete strength class	30	14.5	1.05
BarChip 54 macrofiber	12		640

For discrete reinforcement of concretes, BarChip 54 macrofiber was used. Macrofiber quantities were 0, 3, 5 and 7 kg/m^3. The mechanical properties of macrofibers are indicated in Table 1.

2.2. Test Methods

Compressive strength tests were performed according to EN 12390-3 [18] standard. In these tests, cubic specimens with dimensions of 150 × 150 × 150 mm were used. They were brought to destruction directly between the flat steel plates of the testing machine.

Crack Mouth Opening Displacement (CMOD) tests were conducted as per the requirements of the EN 14651 [19] standard. Specimens in the form of a prism (beam) were used to determine the relationship of force—CMOD. The ratio of height to width (diameter) of specimens was assumed to be 4. The requirements for preparing the specimens have to comply with the BS EN 12390-1 [20] standard. The value of CMOD is the movement of the external faces of the incision made in the center of specimen when it deflects from the loading. The width of the slot on the specimen should not exceed 5 mm and its depth should be 25 mm ± 1 mm.

For laboratory research, the "Toni Technik ToniPRAX" testing machine (Toni Technik Gmbh, Berlin, Germany) was used, which implements uniaxial compression of the specimens with a maximum force of 3000 kN and three-point bending of the specimen with a maximum force of 100 kN. The testing machine must operate in a loading-controlled mode during compressive strength tests and in a displacement-controlled mode during CMOD tests.

For measuring the crack opening during CMOD tests, the high precision displacement transducer "Controls Group P0331/E" (Controls S.P.A., Milan, Italy) was used. This displacement transducer has a measuring capacity of 5 mm and sensitivity of 10^{-3} strain/mm.

The CMOD tests requires the fatigue pre-cracking stage. During this stage, the flexural loading is applied to the specimen at a constant rate of 0.02 mm/s until the Crack Opening Displacement (COD) reached 0.3 mm, after which specimens were subjected to approximately one million cycles of loading. The loading was applied between 10% and 90% of the elastic limit. Frequency was 5 Hz. After the fatigue pre-cracking stage, the specimen was fractured with a constant 0.02 mm/s rate.

Details showing a specimen, supporting and loading system as well as displacement transducer are illustrated in Figure 1.

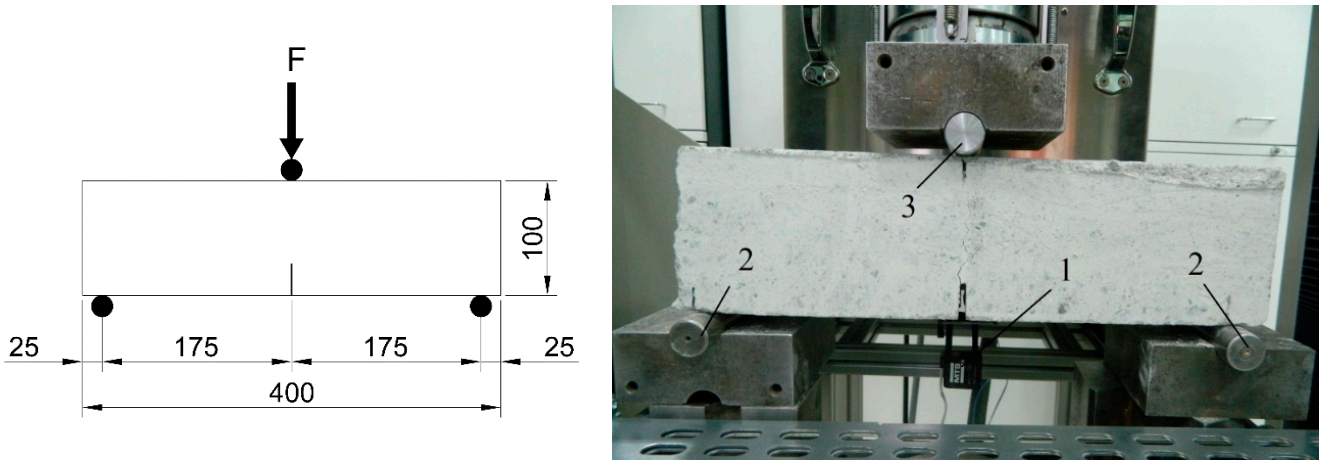

(**a**) (**b**)

Figure 1. Dimensions of a Crack Mouth Opening Displacement (CMOD) test specimen and supporting system (**a**) and general view (**b**) with components on a scale of 1 to 5. 1—CMOD displacements transducer; 2—support rollers; 3—loading roller.

3. Results

The following mechanical properties of non-reinforced concrete were obtained: Young's modulus 30 GPa; compressive strength 25.7 MPa; tension strength 3.8 MPa.

The behavior of concrete under bending is presented in Figure 2.

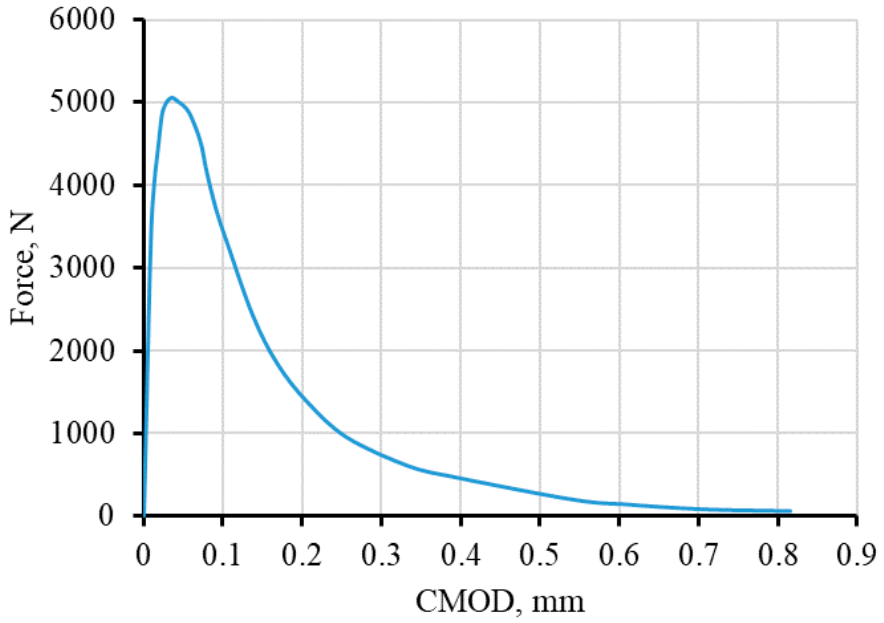

Figure 2. Force versus CMOD from bending test on non-reinforced concrete.

The following mechanical properties of fiber-reinforced concrete were obtained: Young's modulus 30 GPa; compressive strength 28.7 MPa; tension strength 4.2 MPa at a fiber amount of 3 kg/m^3, 4.6 MPa at the fiber amount of 5 kg/m^3 and 5.0 MPa at the fiber amount of 7 kg/m^3.

The behavior of fiber-reinforced concrete under bending is presented in Figure 3.

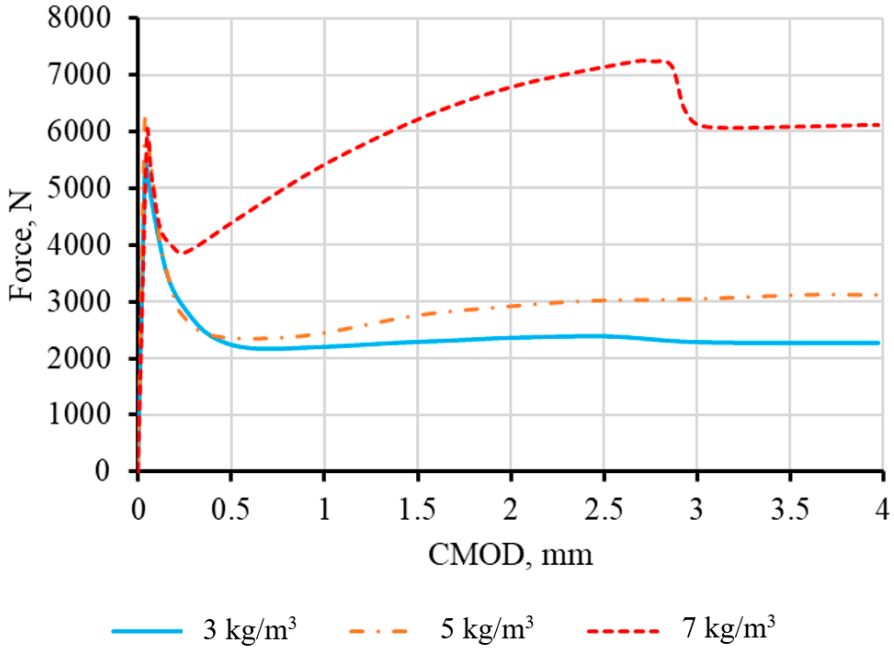

Figure 3. Force versus CMOD from the bending test conducted on the specimen in a form of a beam reinforced by different macrofiber mass amount.

4. Numerical Modeling: Justification of the Model of Fiber-Reinforced Concrete

4.1. General Information about the Model of Plastic Behavior of Concrete with Damage Accumulation (Concrete Damage Plasticity Model)

The concrete damage plasticity model is designed to describe the mechanical behavior of concrete under uniaxial, biaxial and volumetric stress conditions with insignificant values of lateral compression [20–22]. The mechanical behavior of concrete in the model is based on isotropic elastic damage in combination with isotropic plastic behavior for compression and tension that allows describing irreversible deformations in concrete. This approach is suitable because it is assumed that macrofibers in concrete has a chaotic orientation, and due to its sufficiently large content, it is possible for the models to assume the same hardening of concrete in all possible directions. Two main mechanisms of concrete destruction, namely, the formation of separation cracks and plastic destruction under compression, are considered in the model. This approach allows using the model under simple or cyclic static loads or dynamic loads. The model takes into account concrete reinforcement with individual rods, meshes or dispersed reinforcement. The dispersed reinforcement of concrete in the model is set in terms of the amount of energy required for the formation and full opening of a crack.

Parameters used to set the properties of the concrete damage plasticity model with accumulated damages:

- Initial (undamaged) Young's modulus E;
- Poisson's ratio v;
- Ultimate uniaxial compression strength f_{cm};
- Ultimate uniaxial tension strength f_{ctm};
- Diagram of concrete deformations in the axes "force versus CMOD" from bending test (see Figures 2 and 3);
- Dilation angle ψ measured in the p–q plane at high confining pressure. The value should be between 0 and 30 degrees;
- The ratio of initial equibiaxial compressive yield stress to initial uniaxial compressive yield stress α_f. Recommended default value: 1.16 [23];
- Flow potential eccentricity Ie. The eccentricity is a small positive number that defines the rate at which the hyperbolic flow potential approaches its asymptote. Recommended default value: 0.1 [23];

- The ratio of the second stress invariant on the tensile meridian to that on the compressive meridian coefficient of the shape of plastic surface flow K_c. Recommended default value: 0.667 [23].

The values of these parameters were determined based on tests (see Section 3), requirements of regulatory documents, numerical modeling [24–27] as well as recommendations set out in the scientific and technical documents [28–32]. The parameters of the model of plastic behavior of concrete with damage accumulation are summarized in Table 2.

Table 2. Parameters of the model of plastic behavior of concrete with damage accumulation.

Material	*E*, GPa	v	f_{cm}, MPa	f_{ctm}, MPa	ψ	α_f	ϵ	K_c
Non-reinforced B15 concrete strength class	24	0.2	11	0.75	30	1.16	0.1	0.667
Non-reinforced B25 concrete strength class	30	0.2	22	1.05	30	1.16	0.1	0.667
Fiber-reinforced concrete with the fiber amount of 3 kg/m^3								
Fiber-reinforced concrete with the fiber amount of 5 kg/m^3	30	0.2	24	1.05	30	1.16	0.1	0.667
Fiber-reinforced concrete with the fiber amount of 7 kg/m^3								

Damage is usually characterized by the degradation of stiffness. An isotropic scaled damage model from the continuum damage mechanics is introduced in Abaqus to describe the stiffness degradation, which can be represented by Equation (1) under uniaxial loading [23]:

$$\sigma = (1-d)E\left(\varepsilon - \varepsilon^{pl}\right), \quad (1)$$

where σ represents the stress, ε and ε^{pl} represent, respectively, the total and plastic deformation, E represents the initial (undamaged) Young's modulus and d represents the damage factor, which characterizes the degradation of the elastic stiffness and has values in the range between 0 (undamaged) and 1 (fully damaged).

The diagrams in the axes "tensile damage parameter versus CMOD" based on experimental data of CMOD tests are shown in Figure 4. These diagrams are directly used by the concrete damaged plasticity model as additional parameters to correctly simulate the accumulation of damage in concrete.

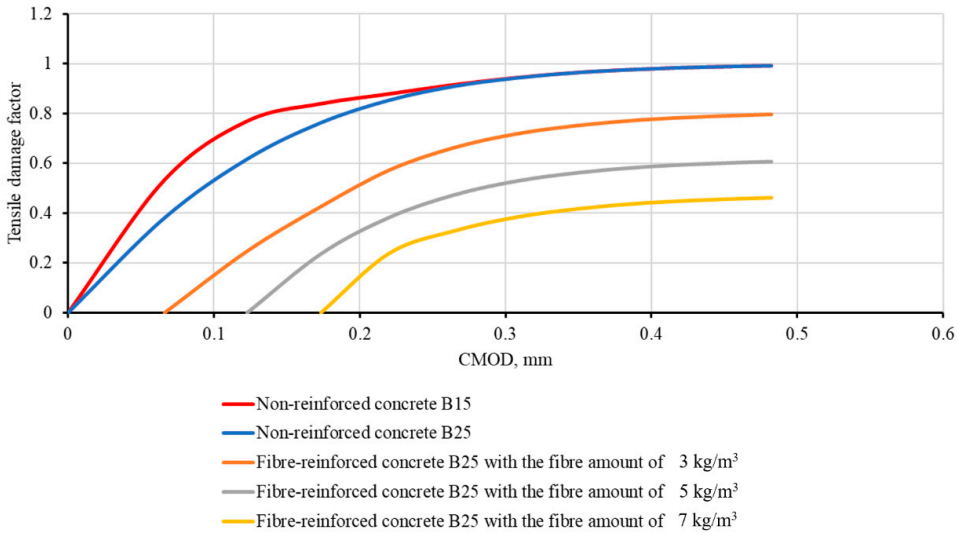

Figure 4. Tensile damage factor versus CMOD according to CMOD test data.

4.2. Determination of Concrete Stress-Strain Diagram under Uniaxial Tension Simulation

The approach of constructing the diagram of the extreme deformation of concrete under uniaxial tension is used based on the results of concrete test under bending. It consists of selecting the parameters of the model of plastic behavior of concrete based on the results of a numerical experiment.

The sequence of selection of damaged concrete plasticity model parameters is shown in Figure 5 as flow chart.

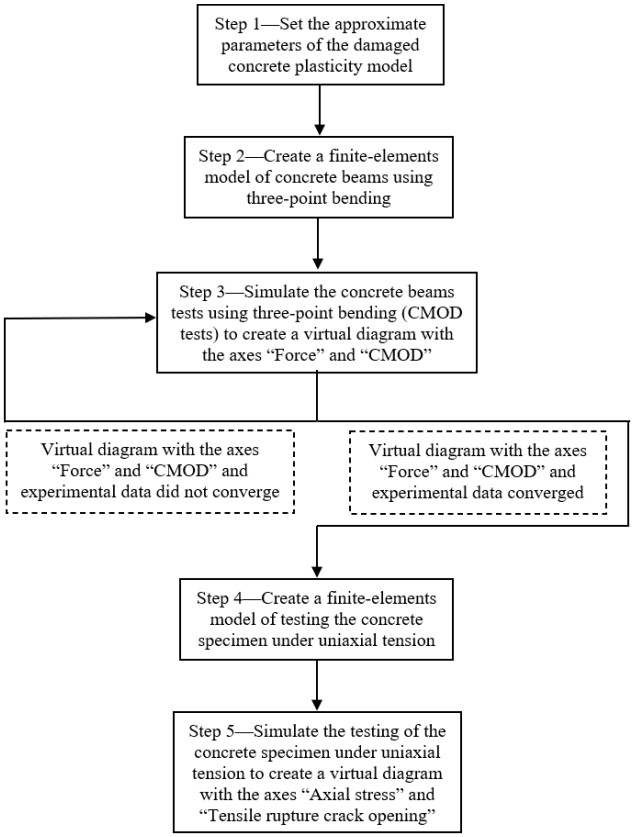

Figure 5. Flow chart of the sequence of selection damaged concrete plasticity model parameters.

The selection of the model parameters sequence includes:

1. Approximate the parameters of the model of plastic behavior of concrete with fracture, which are determined taking into account the data published in scientific papers [23] and experimental data in representation of stress–strain and stress–displacements diagrams of a specific specimen of concrete or fiber-reinforced concrete.
2. Create the finite-elements model of concrete beams using three-point bending to build the virtual experiment.
3. If the results of the virtual experiment differ up to 10% (the peak value of the load at which the crack originates must differ up to 5%) from the experimental laboratory data, then proceed to Step 4. If the condition is not met, the model parameters are corrected and Step 3 of the virtual experiment is repeated.
4. Create the finite-elements model of the concrete specimen under uniaxial tension to build the virtual experiment.
5. Process the obtained data of numerical modeling at Step 4 and present them using the axes "axial stress" and "tensile rupture crack opening."

4.3. Numerical Model of CMOD Tests

The numerical model of concrete under bending (see Figure 6) consists of three separate parts (a concrete beam, two supporting bars and a loading bar). Interaction among parts is carried out through special contact conditions—"hard" contact with friction penalty. A concrete beam is modeled by solid deformable finite elements and it consisted of about 1600 hexagon finite elements of second geometric order. The supporting and loading bars are modeled by finite elements describing an absolutely rigid body.

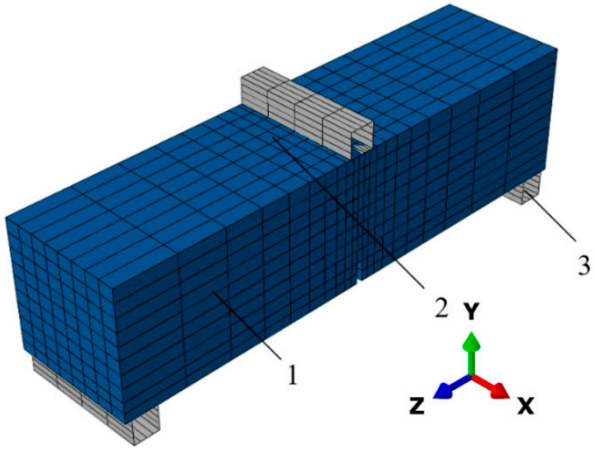

Figure 6. Finite element model for performing a virtual experiment to test a concrete beam using a three-point bend. 1—concrete beam; 2—loading bar; 3—supporting bar.

The dimensions of the beam and the distance between the supporting bars are taken according to the scheme in Figure 1.

The following sequence of numerical experiments is adopted:

- Stage 1—establishing contact interaction among the tested concrete beam, supporting and loading bars;
- Stage 2—transferring the concentrated loading from the bar to the beam. The maximum deflection during the numerical experiment did not exceeded 2 cm. This amount was sufficient to obtain a complete ultimate diagram of the concrete beam deformation.

The diagram in the axes "force" and "CMOD" was constructed based on the test results and compared with the data from laboratory tests under bending (see Figure 7).

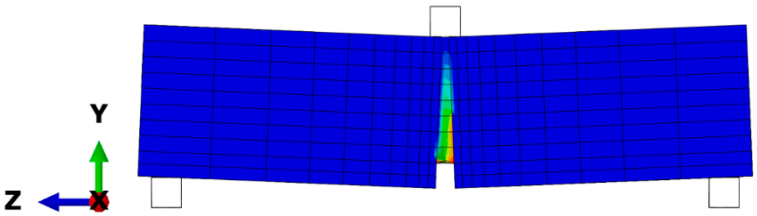

Figure 7. Deformation of a beam using a three-point bending test with the Finite Element Method.

4.4. Numerical Model for the Simulation of Concrete under Uniaxial Tension

The numerical model for testing concrete under uniaxial tension is shown in Figure 8. The following dimensions of the specimen were used during the simulation: 15 × 15 × 55 cm with a weakening area of 10 × 10 × 6 cm at the center. Attenuation in conditions of homogenous uniaxial tension is necessary to localize plastic deformations in a certain area to track the width of the crack opening as well as to specify the area of plastic deformations and accumulation of damage in concrete in an obvious form. In real tests, conventional prism specimens with a cross-sectional area of 10 × 10 mm were used.

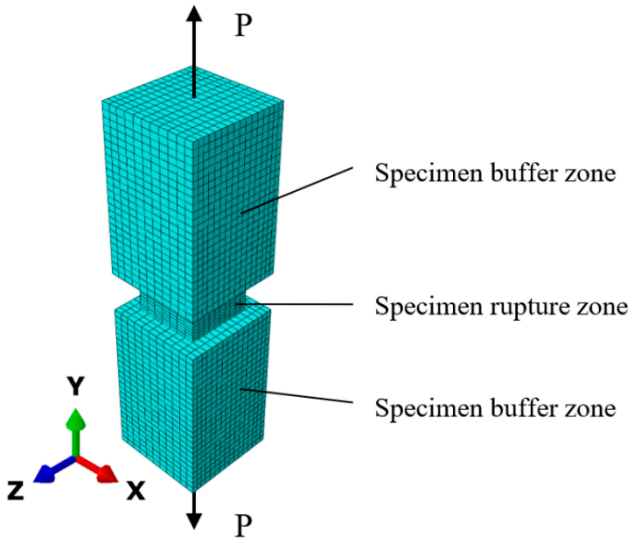

Figure 8. Finite element model for the simulation of concrete under uniaxial tension.

A concrete specimen is modeled by solid deformable finite elements, which consists of about 9850 hexagon finite elements of a second geometric order. Numerical simulation was performed at the following boundary conditions: displacements at the bottom are prohibited in all directions; displacements of the top of the model are prohibited in the horizontal plane; positive forced displacement applied in the vertical direction, which simulate the process of uniaxial tension of concrete specimen. The displacement value was no more than 5 mm, which is sufficient to simulate uniaxial tensile testing of all the materials under consideration (non-reinforced concrete of B15 strength class, non-reinforced concrete of B25 strength class, fiber-reinforced concrete of B25 strength class with a fiber amount of 3, 5 and 7 kg/m^3).

A typical pattern of specimen deformation in a numerical experiment is shown in Figure 9.

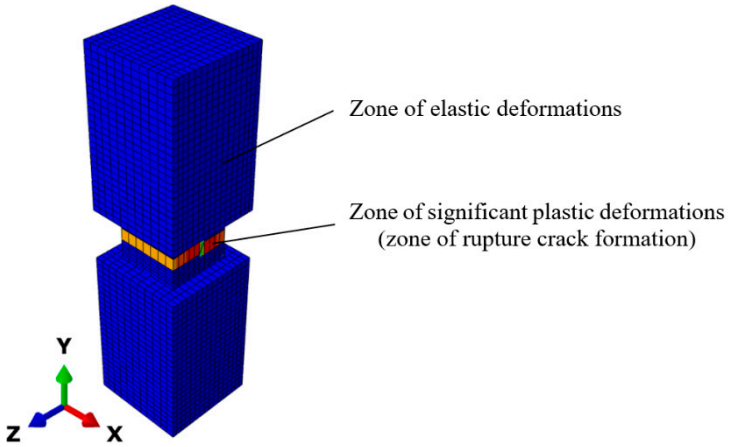

Figure 9. Deformation of a concrete specimen under uniaxial tension based on numerical modeling.

Based on the test results the diagrams were performed in the axes "axial stress" and "tensile rupture crack opening." These diagrams are shown in Figure 10. They are used as a basis for obtaining the diagrams shown in Figure 4.

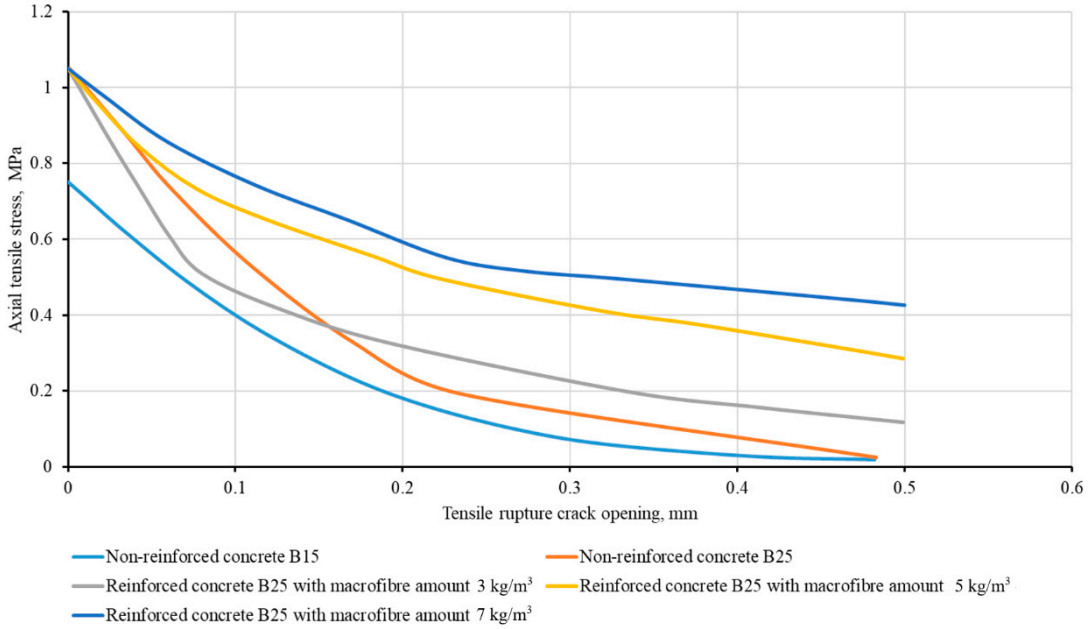

Figure 10. Uniaxial tensile stress versus tensile rupture crack opening according to concrete specimen fracturing simulation.

5. Numerical Simulation of Interaction of Tunnel Lining with Rock Mass under Seismic Loading

The numerical simulation was performed in the framework of setting a plane strain in the Simulia Abaqus software package. The general design scheme included in the model is shown in Figure 11.

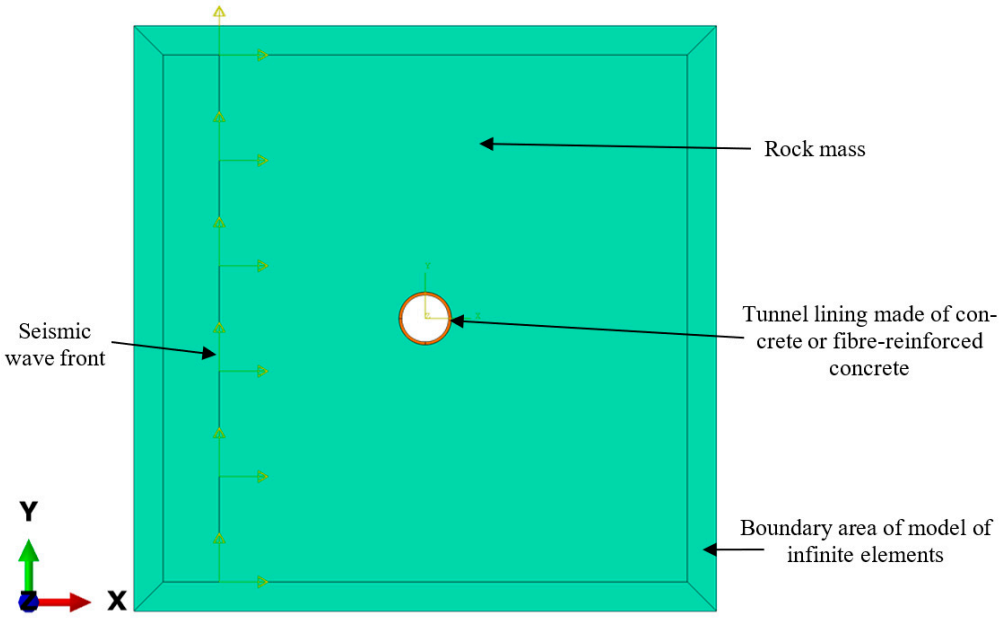

Figure 11. Design scheme of the finite element model.

Calculations on the numerical model were implemented in two stages. Simulation of geostatic loading formation in the tunnel lining from the self-weight of the host rock mass was performed in Stage-1. In Stage-2, the simulation of a seismic impact propagating as a wave disturbance through the calculated area of the rock mass was performed.

The model of a linearly deformable body with the parameters presented in Table 3 was used as a mechanical model of a rock mass. Modeling of the behavior of concrete and

fiber-reinforced concrete of the tunnel lining was performed using the Damaged Concrete Plasticity model. Model parameters were determined based on laboratory tests data and they are summarized in Table 2.

Table 3. Physical and mechanical properties of rocks [15].

Name	Density, kN/m^3	Deformation Properties		The Parameters of Rayleigh Damping	
		Young's Modulus E, GPa	Poisson's Ratio ν	α	β
Mass of Urtites	0.025	30	0.2	0.037	0.0009

The boundary conditions on the finite element model were formulated in a specific way to correctly model the seismic impact. The boundary area of the model was divided by a single layer of infinite elements, the main task of which was to extinguish the seismic wave passing through the model boundary. Thus, the effect of wave reflection from the boundary and subsequent related phenomena, such as the possible interference of direct and reflected seismic waves, were excluded.

The parameters of the natural stress state of the host rock mass were determined, taking into account the estimated tunnel depth of 120 m.

The seismic impact was modeled by applying forced accelerations on the inner face of the model, set component-by-component for the directions of the axes of the coordinate system. The accelerogram of a real earthquake that occurred in Friuli in 1976 shows a magnitude of about 6.5. The component-by-component decomposition of this accelerogram is shown in Figure 12.

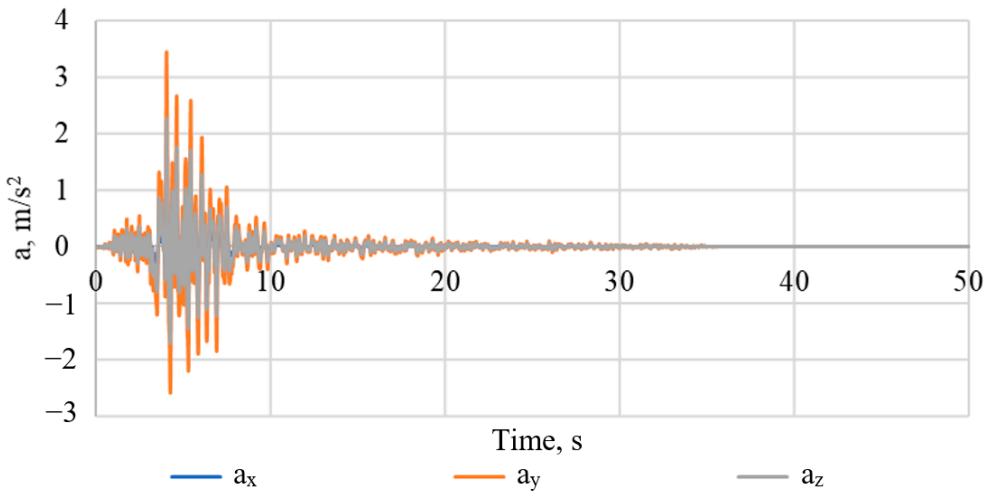

Figure 12. Calculated accelerogram of seismic impact.

The main task of modeling was to state the dependencies of the damage formation in the concrete lining during its dynamic loading under the calculated seismic impact as well as to identify the influence of fiber amount in concrete on its resistance to the accumulation of these damages. To solve this problem, all calculations were performed under the same conditions for the variants when the tunnel lining is made of non-reinforced concrete and of fiber-reinforced concrete with the fiber amount of 3, 5 and 7 kg/m^3.

The calculated zones of material damage of the tunnel lining under seismic impact at different time intervals are shown in Figure 13, provided that the tunnel lining is made of non-reinforced monolithic concrete or from fiber-reinforced concrete with a polypropylene macrofiber amount of 3, 5 and 7 kg/m^3. The quantitative damage indicator shows how much of the initial strength and stiffness is lost by concrete in the current time interval due to the crack development.

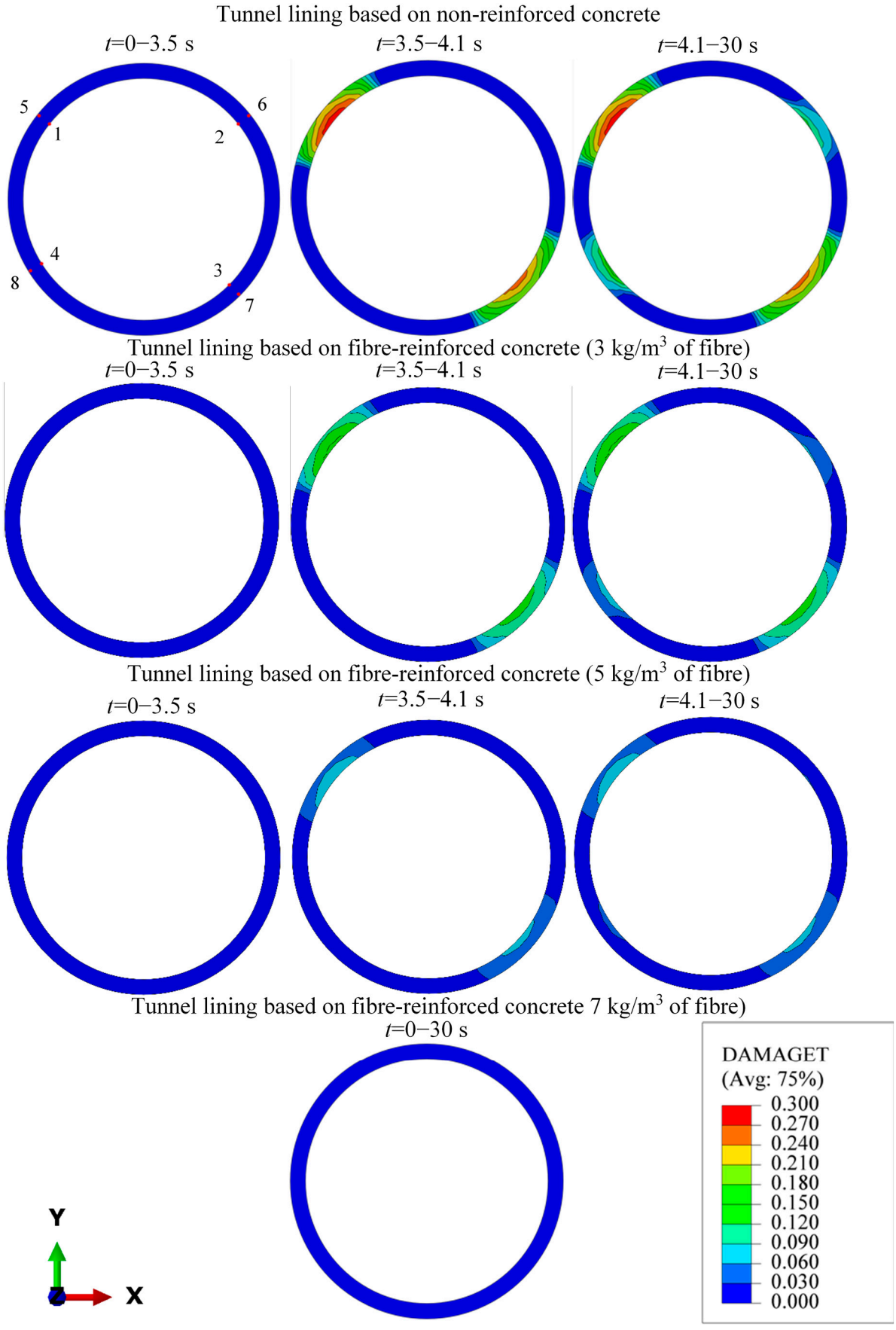

Figure 13. Patterns of formation of damage zones in the tunnel lining material under seismic load.

Seismic impact from an earthquake causes the formation of breakaway cracks in the lining of non-reinforced monolithic concrete due to the appearance of significant tensile stresses in certain parts of the lining at particular time intervals.

The location and numbering of the characteristic points of the tunnel lining are shown in Figure 12. The curves of changes of the highest and lowest principal stresses at the characteristic points of the tunnel lining made of non-reinforced monolithic concrete are shown in Figure 14.

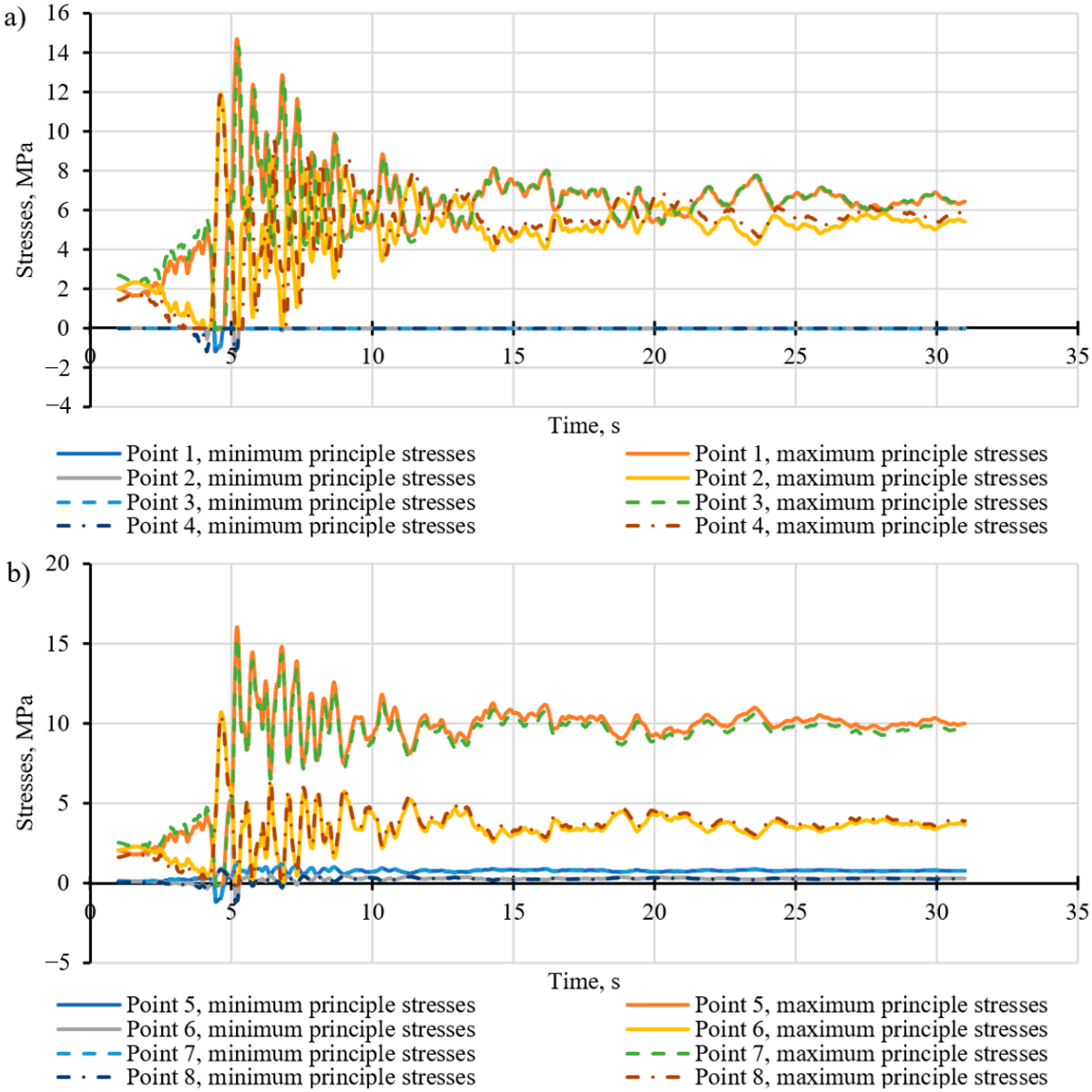

Figure 14. Curves of the maximum and minimum principal stresses in the tunnel lining made of non-reinforced concrete under seismic load for the points of the inner contour (**a**) and the outer contour (**b**).

The analysis of changes of the stress state of the tunnel lining at characteristic points over time allows confirming the assumption about the formation of tensile stress in zones of damage appearing before damage accumulation. The compressive stress is not high enough to cause the material damage.

The curves' damage accumulation at the characteristic points of the tunnel lining over time are shown in Figure 15.

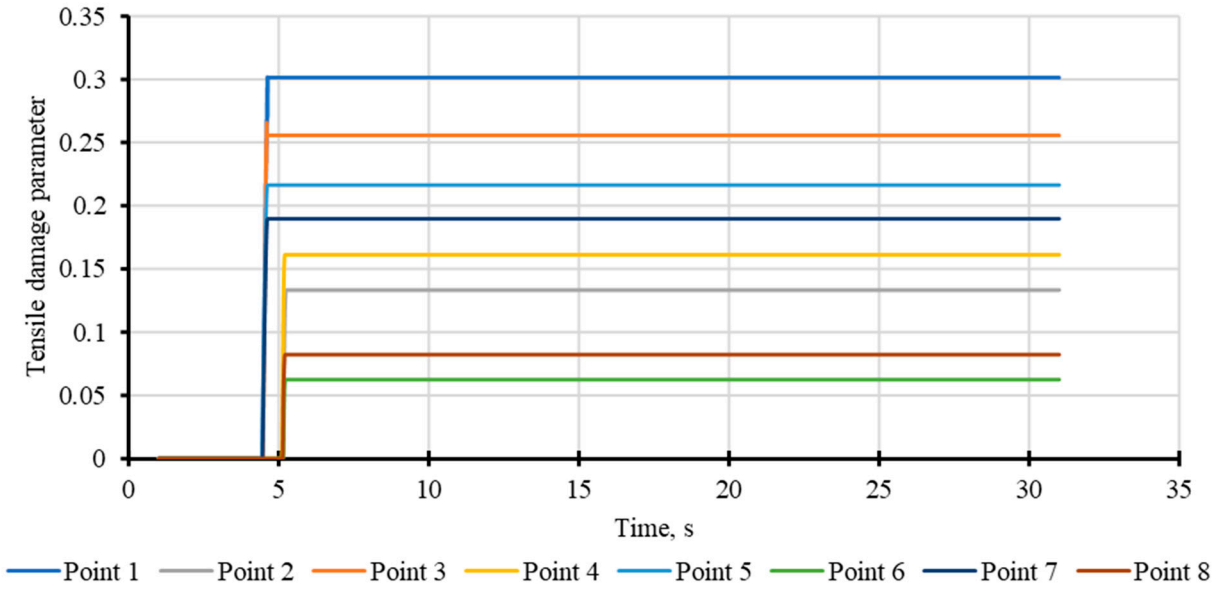

Figure 15. Damage accumulation curves in the tunnel lining material at characteristic points.

The localization of damage zones and the sequence of their formation over time were stated as a result of modeling. First of all, the zones of greatest damage with length about 3.5 m are formed in the lining along the tunnel contour. The zones are located symmetrically relative to the tunnel axis at the angle about 45° counter clockwise to the vertical. Second, the formation of damage zones with a length of about 2.5 m occurs along the tunnel contour. The zones are located symmetrically relative to the tunnel axis at the angle about 50° clockwise to the vertical. Thus, the lining of non-reinforced monolithic concrete as a result of the calculated seismic impact from an earthquake is not destroyed, but the accumulation of structural defects occurs in the form of separation cracks, which locally weaken the rigidity and load-bearing capacity of the lining by 8–30% relative to the initial indicators. Most likely, repair work to eliminate the separation cracks formed in the material [33–37] would be required in the tunnel lining in such conditions in practice.

Calculations of tunnel lining made of fiber-reinforced concrete with polymer macrofiber amount of 7 kg/m^3 show that the presence of a sufficient amount of fiber in the concrete composition allows avoiding damage in the tunnel lining under dynamic loading. The fiber amount of less than 7 kg/m^3, namely 3 and 5 kg/m^3, reduces the level of damage to the lining structure after seismic impact. This can be explained by the fact that the presence of fiber increases the total amount of energy that must be spent on concrete destruction in comparison with non-reinforced concrete of the same class of compressive strength. This can significantly increase the seismic resistance of the tunnel lining. In practice, repair work in the tunnel after a seismic impact not exceeding the calculated magnitude would not be required if the lining made of fiber-reinforced concrete with the fiber amount of 7 kg/m^3 was used, since separation cracks in the structure of the lining material are not formed.

6. Conclusions

The results of the laboratory tests of the specimen made of concrete and fiber-reinforced concrete justifies the parameters of the model of plastic behavior of concrete with damages accumulation. In this paper, the method of substantiating the parameters of mechanical models of materials based on performing virtual tests of specimens is shown and applied.

Calculations in the framework of a numerical model of the seismic impact on a tunnel lining made of concrete or fiber-reinforced concrete allowed describing the mechanism of damage formation in the form of separation cracks as well as confirming the effectiveness of using fiber-reinforced concrete in structures operating under dynamic loading.

Calculations of tunnel lining made of fiber-reinforced concrete with the polymer macrofiber amount of 7 kg/m^3 show that the presence of the sufficient amount of fiber in

concrete composition makes it possible to completely avoid damage in the tunnel lining under dynamic loading. A fiber amount of less than 7 kg/m^3, namely 3 and 5 kg/m^3, reduces the damage level of lining structure after seismic impact.

In our view, the subsequent development of future research lies in multivariate modeling of the work of building structures in a spatial setting under dynamic loads to identify general patterns for determining the optimal amount of polymer fiber in concrete.

Author Contributions: Conceptualization, N.B. and O.S.; methodology, N.B., A.A. and H.T.; validation, O.S. and H.T.; investigation N.B., O.S. and A.A.; writing—original draft preparation, N.B.; writing—review and editing, O.S. and H.T.; supervision, N.B.; project administration, O.S. and A.A. All authors have read and agreed to the published version of the manuscript.

Funding: This research received no external funding.

Institutional Review Board Statement: Saint-Petersburg Mining University, protocol code 2020-12-01cfrom 14.12.2020.

Informed Consent Statement: Informed consent was obtained from all subjects involved in the study.

Data Availability Statement: Data is contained within the article.

Conflicts of Interest: The authors declare no conflict of interest.

References

1. Zhu, H.; Yu, K.; Li, V.C. Sprayable engineered cementitious composites (ECC) using calcined clay limestone cement (LC3) and PP fiber. *Cem. Concr. Compos.* **2021**, *115*, 103868. [CrossRef]
2. Li, L.; Cai, Z.; Yu, K.; Zhang, Y.; Ding, Y. Performance-based design of all-grade strain hardening cementitious composites with compressive strengths from 40 MPa to 120 MPa. *Cem. Concr. Compos.* **2019**, *97*, 202–217. [CrossRef]
3. Klyuev, S.; Klyuev, A.; Vatin, N. Fiber concrete for the construction industry. *Mag. Civ. Eng.* **2018**, *84*, 41–47. [CrossRef]
4. Heravi, A.A.; Smirnova, O.; Mechtcherine, V. Effect of strain rate and fiber type on tensile behavior of high-strength strain-hardening cement-based composites (HS-SHCC). In *Strain-Hardening Cement-Based Composites, Proceedings of the International Conference on Strain-Hardening Cement-Based Composites, Dresden, Germany, 18–20 September 2017*; Springer: Berlin/Heidelberg, Germany, 2017; Volume 15, pp. 266–274.
5. Chaudhari, S.V.; Chakrabarti, M.A. Modeling of Concrete for Nonlinear Analysis using Finite Element Code ABAQUS. *Int. J. Comput. Appl.* **2012**, *44*, 14–18. [CrossRef]
6. Mihai, I.C.; Jefferson, A.; Lyons, P. A plastic-damage constitutive model for the finite element analysis of fiber reinforced concrete. *Eng. Fract. Mech.* **2016**, *159*, 35–62. [CrossRef]
7. Sitek, M.; Adamczewski, G.; Szyszko, M.; Migacz, B.; Tutka, P.; Natorff, M. Numerical Simulations of a Wedge Splitting Test for High-strength Concrete. *Procedia Eng.* **2014**, *91*, 99–104. [CrossRef]
8. Arain, M.F.; Wang, M.; Chen, J.; Zhang, H. Experimental and numerical study on tensile behavior of surface modified PVA fiber reinforced strain-hardening cementitious composites (PVA-SHCC). *Constr. Build. Mater.* **2019**, *217*, 403–415. [CrossRef]
9. Karasev, M.A.; Sotnikov, R.O.; Sinegubov, V.Y.; Egorova, N.A.; Makarov, K.V.; Thorikov, A.I. Development of a model for predicting the dynamic effect on the stability of rock excavation. *J. Physics Conf. Ser.* **2019**, *1384*, 012051. [CrossRef]
10. Protosenya, A.G.; Iovlev, G.A. Prediction of spatial stress-strain behavior of physically nonlinear soil mass in tunnel face area. *MIAB Min. Informational Anal. Bull.* **2020**, *5*, 128–139. [CrossRef]
11. Trushko, V.L.; Protosenya, A.G. Prospects of geomechanics development in the context of new technological paradigm. *ЗапискиГорного института* **2019**, *236*, 162–166. [CrossRef]
12. Trushko, O.V.; Trushko, V.L.; Demenkov, P.A. Arrangement of Multistory Underground Parking Garages in Complex Engineering and Geological Environment. *Int. J. Math. Eng. Manag. Sci.* **2020**, *5*, 897–912. [CrossRef]
13. Potemkin, D.A.; Popov, M.G.; Trushko, O.V. Examination and analysis of actual stability of mine workings at the Yakovlevsky iron ore deposit. *ARPN J. Eng. Appl. Sci.* **2018**, *13*, 2490–2499.
14. Chi, T.N.; Gospodarikov, A. Hyperstatic reaction method for calculations of tunnels with horseshoe-shaped cross-section under the impact of earthquakes. *Earthq. Eng. Eng. Vib.* **2020**, *19*, 179–188. [CrossRef]
15. Kotikov, D.A.; Shabarov, A.N.; Tsirel, S.V. Connecting seismic event distribution and tectonic structure of rock mass. *Gorn. Zhurnal* **2020**, *2020*, 28–32. [CrossRef]
16. Kholodilov, A.N.; Gospodarikov, A.P. Modeling Seismic Vibrations under Massive Blasting in Underground Mines. *J. Min. Sci.* **2020**, *56*, 29–35. [CrossRef]
17. Kazanin, O.I.; Sidorenko, A.A.; Sirenko, Y.G. Numerical study of the air-gas dynamic processes when working out the Mosshny seam with longwall faces. *ARPN J. Eng. Appl. Sci.* **2018**, *13*, 1534–1538.

18. British Standards Institution. BS EN 12390-3:2019 Testing Hardened Concrete. *Compressive Strength of Test Specimens.* 2019. Available online: https://standards.iteh.ai/catalog/standards/cen/7eb738ef-44af-436c-ab8e-e6561571302c/en-12390-3-2019 (accessed on 26 January 2021).
19. British Standards Institution. BS EN 14651:2005 Test Method for Metallic Fibre Concrete—Measuring the Flexural Tensile Strength (Limit of Proportionality (LOP), Residual). 2005. Available online: https://standards.iteh.ai/catalog/standards/cen/29609539-5a5d-498b-91fe-23fffef25d89/en-14651-2005 (accessed on 26 January 2021).
20. British Standards Institution. BS EN 12390-1:2012 Testing Hardened Concrete. *Shape, Dimensions and Other Requirements for Specimens and Moulds.* 2012. Available online: https://shop.bsigroup.com/ProductDetail?pid=000000000030397528 (accessed on 26 January 2021).
21. Dulinska, J.M.; Murzyn, I.J. Dynamic behavior of a concrete building under a mainshock–aftershock seismic sequence with a concrete damage plasticity material model. *Geomat. Nat. Hazards Risk* **2016**, *7*, 25–34. [CrossRef]
22. Hafezolghorani, M.; Hejazi, F.; Vaghei, R.; Bin Jaafar, M.S.; Karimzade, K. Simplified Damage Plasticity Model for Concrete. *Struct. Eng. Int.* **2017**, *27*, 68–78. [CrossRef]
23. Nascimento, M. *ABAQUS 6.14 Analysis User's Guide*; Dassault Systemes Simulia Corp.: Providence, RI, USA, 2014.
24. Farahmandpour, C.; Dartois, S.; Quiertant, M.; Berthaud, Y.; Dumontet, H. A concrete damage–plasticity model for FRP confined columns. *Mater. Struct.* **2017**, *50*, 1521. [CrossRef]
25. Cheng, H.; Paz, C.M.; Pinheiro, B.C.; Estefen, S.F. Experimentally based parameters applied to concrete damage plasticity model for strain hardening cementitious composite in sandwich pipes. *Mater. Struct.* **2020**, *53*, 1–17. [CrossRef]
26. Wahalathantri, B.; Thambiratnam, D.; Chan, T.; Fawzia, S. A material model for flexural crack simulation in reinforced concrete elements using ABAQUS. In *Proceedings of the First International Conference on Engineering, Designing and Developing the Built Environment for Sustainable Wellbeing*; Queensland University of Technology: Brisbane, QLD, Australia, 2011; pp. 260–264.
27. Popov, V.; Morozov, V.; Pukharenko, Y.; Plyusnin, M.G. Consideration of Variability of Concrete Characteristics in Calculation of Reinforced Concrete Structures. *Mater. Sci. Forum* **2016**, *871*, 166–172. [CrossRef]
28. Kharitonov, A.; Ryabova, A.; Pukharenko, Y. Modified GFRC for Durable Underground Construction. *Procedia Eng.* **2016**, *165*, 1152–1161. [CrossRef]
29. Seok, S.; Haikal, G.; Ramirez, J.A.; Lowes, L.N.; Lim, J. Finite element simulation of bond-zone behavior of pullout test of reinforcement embedded in concrete using concrete damage-plasticity model 2 (CDPM2). *Eng. Struct.* **2020**, *221*, 110984. [CrossRef]
30. Batalha, N.; Rodrigues, H.; Varum, H. Seismic performance of RC precast industrial buildings—learning with the past earthquakes. *Innov. Infrastruct. Solutions* **2018**, *4*, 4. [CrossRef]
31. Furtado, A.; Rodrigues, H.; Arêde, A.; Varum, H.; Grubišić, M.; Šipoš, T.K. Prediction of the earthquake response of a three-storey infilled RC structure. *Eng. Struct.* **2018**, *171*, 214–235. [CrossRef]
32. Benin, A.; Guzijan-Dilber, M.; Diachenko, L.; Semenov, A. Finite element simulation of a motorway bridge collapse using the concrete damage plasticity model. *E3S Web Conf.* **2020**, *157*, 06018. [CrossRef]
33. Shuaib, M.F.; Ibrahim, H.H.; Abbass, A. Repair and Strengthening of Underground Structures. In Proceedings of the Workshop of "Underground Structures in Hot Climate Conditions", Riyadh, Saudi Arabia, 8–9 December 2009.
34. Hashash, Y.M.A.; Hook, J.J.; Schmidt, B.; Yao, J.I.-C. Seismic design and analysis of underground structures. *Tunn. Undergr. Space Technol.* **2001**, *16*, 247–293. [CrossRef]
35. Pérez, E.S.; Menéndez-Pidal, I.; Galindo, R.; López-Querol, S.; Pascual-Arribas, C. Historical earthquake parameters by geological and seismic site analysis: The 1908 Cerbón earthquake (Spain). *Bull. Int. Assoc. Eng. Geol.* **2016**, *75*, 1251–1271. [CrossRef]
36. Nuguzhinov, Z.; Vatin, N.; Bakirov, Z.; Khabidolda, O.; Zholmagambetov, S.; Kurokhtina, I. Stress-strain state of bending reinforced beams with cracks. *Mag. Civ. Eng.* **2020**, *96*, 1–15.
37. Barabanshchikov, Y.G.; Belkina, T.V.; Semenov, K.V.; Zimin, S.S.; Akimov, S.V.; Vatin, N.I. Reasons of cracks in floor slab panel. *IOP Conf. Series Mater. Sci. Eng.* **2020**, *896*, 012068. [CrossRef]